Title
CHARGE-EXCHANGE REACTION (d, He)

Author
Stahel, D.P.

Publication Date
1979-05-01

Lawrence Berkeley Laboratory

UNIVERSITY OF CALIFORNIA, BERKELEY, CA

Submitted to Physical Review C

CHARGE-EXCHANGE REACTION (d,^{2}He)

D. P. Stahel, R. Jahn, G. J. Wozniak and
Joseph Cerny

May 1979

Prepared for the U. S. Department of Energy
under Contract W-7405-ENG-48

DISCLAIMER

CHARGE-EXCHANGE REACTION (d, ^{2}He)

D. P. Stahel, R. Jahn[†], G. J. Wozniak and Joseph Cerny

Lawrence Berkeley Laboratory and
Department of Chemistry
University of California
Berkeley, California 94720

May, 1979

ABSTRACT

^{2}He energy spectra were obtained for the (d, ^{2}He) reaction on targets of ^{6}Li, ^{10}B, and ^{12}C at E_d = 55 MeV in a kinematically complete coincidence measurement of two protons with small relative energies. Projected proton energy spectra show an enhancement of the cross section over phase space due to the final-state interaction between two protons in a relative $^1S_0$ state. ^{2}He angular distributions were found to be in reasonable agreement with predictions of microscopic DWBA calculations using spectroscopic amplitudes derived from intermediate-coupling wave functions.

[NUCLEAR REACTIONS ^{6}Li, ^{10}B, ^{12}C(d, ^{2}He), E_d = 55 MeV; measured $\sigma(E_f, \Theta)$, microscopic DWBA analysis.]

I. INTRODUCTION

The feasibility of detecting the unbound ^{2}He system as a nuclear reaction product has recently been demonstrated in the study of the $(\alpha,{}^{2}He)$ reaction on several light nuclei.[1] Utilization of this experimental approach opens up a wide range of new nuclear reactions which can be used for the study of nuclear structure and reaction mechanisms. Among these reactions, that of charge-exchange via $(d,{}^{2}He)$ is of particular interest. Such studies should be a useful complement to other charge-exchange reactions producing neutron-excess nuclei, such as the (n,p), $(t,{}^{3}He)$ and heavy-ion induced reactions, many of which have experimental problems associated with their general application. For example, high-energy neutron beams have poor energy resolution and low intensities whereas triton beams are currently only available at moderate energies ($<$ 25 MeV). Though heavy-ion reactions (e.g., $({}^{7}Li,{}^{7}Be)$) are being increasingly employed, the presence of bound excited states of the ejectile frequently complicates the interpretation of the spectra. Since intense high energy deuteron beams are readily available and there are no bound states in ^{2}He, the $(d,{}^{2}He)$ reaction was investigated for its promise as a charge-exchange reaction.

From the theoretical point of view, the $(d,{}^{2}He)$ reaction differs from charge-exchange reactions induced by spin 1/2 projectiles, such as the (n,p) reaction, in that the latter reaction may proceed by both spin-flip (S = 1) and non-spin-flip (S = 0) transitions whereas the $(d,{}^{2}He)$ reaction is always restricted to spin-flip transitions. Thus, the $(d,{}^{2}He)$ reaction is only governed by the $V_{11}(\vec{\sigma}\cdot\vec{\sigma})(\vec{\tau}\cdot\vec{\tau})$ part of the effective nuclear interaction, whereas in the (n,p) reaction in addition the $V_{01}(\vec{\tau}\cdot\vec{\tau})$ part can contribute to some transitions. Therefore, every state populated in the (d,^{2}He) reaction should also be seen in the corresponding (n,p) reaction; on the other hand, if transitions, which are observed strongly in the (n,p) reaction, are unobserved or only weakly observed in the (d,^{2}He) reaction, this may indicate that they are favored with S = 0 but unfavored with S = 1. Thus by comparing the levels populated in the same final nucleus by these two reactions, one may learn something about the character of these final states.

Owing to the scarcity of high energy (n,p) data which could be used for comparative purposes, the (d,^{2}He) reaction was initially studied at E_d = 55 MeV on the T_z = 0 targets ^{6}Li, ^{10}B and ^{12}C producing T_z = 1 final nuclei, since in these cases the energy spectra can also be directly compared with those from reactions such as (p,n) which produce the T_z = − 1 mirror nuclei.

In Sec. II, the ^{2}He detection system and the experimental method are presented. A discussion of the measured energy spectra is given in Sec. III and Sec. IV presents the results of a microscopic distorted-wave Born-approximation (DWBA) analysis of the angular distributions from the (d,^{2}He) reaction on ^{10}B and ^{12}C.

II. EXPERIMENTAL PROCEDURE

A. ^{2}He detection system

It is well known that ^{2}He (the di-proton) does not have any bound states. However, in many reactions producing ^{2}He as a residual nucleus such as the ^{3}He(d,t)^{2}He and ^{2}H(p,n)^{2}He reactions[2-4] an enhancement of the cross section at small relative pp energies ε has been observed, which is attributed to the pp final-state interaction (FSI) of the virtual (or anti-bound) $^{1}S_{0}$ state of ^{2}He. This enhancement peaks at $\varepsilon \approx 400$ keV. For smaller values of ε the Coulomb repulsion begins to dominate and counteracts the attractive nuclear interaction. For larger values of ε, the effects of the FSI fall off fairly slowly; they are noticeable up to several MeV in relative energy.

Detection of ^{2}He as an outgoing system requires a coincidence measurement of two protons with small relative energies, for which the FSI enhancement is the greatest. Since the relative pp energy ε is given by

$$\varepsilon = \frac{1}{2}\left(E_1 + E_2 - 2\sqrt{E_1E_2}\cos\Theta_{12}\right) \tag{1}$$

where E_1 and E_2 are the laboratory energies of the two protons, it is necessary that the angle Θ_{12} between the directions of the two protons, and thus the angular separation between the two counters, be of the order of only a few degrees.

Figure 1 shows a schematic diagram of the ^{2}He detection system. It consisted of two large solid angle ΔE-E counter telescopes collimated by 8 mm wide and 10 mm high slits which were separated vertically by 10 mm. At 11 cm distance from the target, this system permitted the detection of pp events with $\Theta_{12} = 5^{\circ} - 15^{\circ}$. The ΔE counters were phosphorus diffused silicon, 380 μm thick, and the E detectors were Si(Li), 5 mm thick, all having the same area of $1 \times 1.4\ cm^2$. In addition, 5 mm thick counters were mounted behind the E detectors in order to reject events that traversed the ΔE-E system.

Each counter was connected to a charge-sensitive preamplifier whose slow output was fed into a high-rate linear amplifier. Both ΔE-preamplifiers additionally produced fast pick-off signals which were run into constant-fraction discriminators (CFD) whose fast outputs were used as "start" and "stop" signals for a time-to-amplitude converter (TAC). The output signal of the TAC is proportional to the time-of-flight difference (ΔTOF) between the particles being detected in the separate telescopes. By applying a high bias voltage (2 V/μm) on the ΔE detectors to minimize the charge collection time and by using low capacity cables, a time resolution of about 200 ps (FWHM) was obtained as measured with a fast rise-time pulser. The fast CFD output signals were also run into fast pile-up rejectors which permitted a high count rate ($\sim 3 \times 10^4$/s) in each ΔE counter with an associated system deadtime of about 20%.

The two ΔE and two E signals were gated by the TAC signal such that any two particles in coincidence within one beam burst (or two sequential beam bursts for background analysis) were accepted. These four signals together with the TAC signal were transmitted to a ModComp IV computer and subsequently written on magnetic tape event-by-event for later analysis.

Although events corresponding to any two particles arriving at the two ΔE counters within 200 ns were stored on tape, during both the data acquisition process and the off-line analysis, particle identification (PI) spectra were generated using the algorithm $PI \propto (E+\Delta E)^{1.73} - E^{1.73}$ in order to select two proton events only. Furthermore a narrow gate was set in the TAC spectrum such that only events with $|\Delta TOF| \leqslant 1.5$ ns were accepted, as indicated with vertical arrows in the ΔTOF spectrum from the $^{12}C(d,{}^{2}He)^{12}B$ (g.s.) reaction shown in Fig. 2. The contribution from random coincidences within this gate was determined by setting an equally wide gate around the peak arising from purely random coincidence events between one proton and a second one from the following beam burst. In order to correct for these random coincidence events, all energy spectra were generated first with the real, then with the random TAC gates; finally the latter was subtracted from the former. Since there is a large proton flux associated with the high energy deuteron beam, the random coincidence contribution was reduced by limiting the singles count rate in each ΔE detector to about 2×10^4/s. The deadtime and stability of the electronic system were continuously checked with pulser signals which were triggered by a monitor counter and injected at the preamplifiers.

B. Experimental method

These experiments were performed using a 55 MeV deuteron beam from the Lawrence Berkeley Laboratory 88-inch cyclotron. For each target and angle, the beam current was adjusted to maintain a singles count rate in the ΔE counters of about 2×10^4/s. Beam intensities on target ranged from 30 nA at forward angles to 160 nA at backward angles. Self supporting targets of ^{6}Li(99% enriched, 300 μg/cm^2), ^{10}B (98% enriched, 155 μg/cm^2) and ^{12}C (natural, 310 μg/cm^2) were mounted on a target ladder in the center of a 51 cm diameter scattering chamber whose pressure was kept at 2×10^{-5} Torr. Unscattered beam was collected in a Faraday cup which was connected to a current integrator to measure the total charge of beam particles which passed through the target.

III. EXPERIMENTAL RESULTS

A. Energy spectra

Figure 3 shows a two-dimensional spectrum of the total laboratory energies E_{p_1} vs. E_{p_2} of two protons which arrived at the ΔE counters within 1.5 ns, produced in the bombardment of a ^{12}C target with 55 MeV deuterons. The ^{2}He detector system was set at $\Theta_{lab} = 15^{\circ}$ for which the spherical polar angles of the center of each telescope are $\Theta_1 = \Theta_2 = 30.4^{\circ}$ and $\Delta\phi = 19.8^{\circ}$. The solid lines represent the kinematic loci for the (d,pp) reaction leaving ^{12}B in its ground state (g.s.) or in one of its excited states. They were calculated with the three-body kinematics formalism given by Ohlsen.[5] The dashed lines represent all the points of E_{p_1} and E_{p_2} for which ε has a constant value. They were evaluated for ε = 0.2, 0.4 and 1.0 MeV and are shown only on one side of the $E_{p_1} = E_{p_2}$ line since the spectrum is symmetric about this line. The experimental data clearly show the FSI enhancement of the cross section at small relative pp energies.

In analyzing such data it is convenient to project each kinematic locus onto the E_{p_1}-axis. A proton energy spectrum $d^3\sigma/d\Omega_1 d\Omega_2 dE_{p_1}$ created in this way is presented in Fig. 4 for the (d,pp) reaction leading to the ^{12}B g.s. It should be noted that the ε-scale inserted in this figure is nonlinear as a function of E_{p_1}. Drawn as a solid line is the result of a Watson-Migdal FSI calculation[6,7] using a scattering length $a = -7.82$ fm and an effective range $r_{eff} = 2.81$ fm, which are standard values deduced from low energy pp scattering and FSI analyses.[8] The calculation reproduces quite well the shape of the spectrum and clearly exhibits the FSI enhancement over the almost flat phase space distribution. In order to emphasize the fact that the detection system employed selects the region of phase space in which the effects of the pp FSI arising from the virtual $^1S_0$ g.s. of ^{2}He are important, the (d,pp) reactions will henceforth be denoted as the (d,^{2}He) reaction.

A ^{2}He energy spectrum can be created by projecting a two-dimensional spectrum (Fig. 3) onto the diagonal line $E_{p_1} = E_{p_2}$, since in the present reactions the kinematic loci are almost straight lines perpendicular to the diagonal line (and do not possess a lower branch of the kinematical solution). Thus for a given state in the recoil nucleus the sum of $E_{p_1} + E_{p_2} = E_{^2He}$ has a nearly constant value. ^{2}He energy spectra obtained this way are shown in Figs. 5-7. The contribution of the curvature of the kinematic loci to the peak widths observed in these spectra is quite small; the widths of the peaks are primarily determined by the variation of $E_{^2He}$ over the horizontal acceptance angle of 4°.

B. Absolute ^{2}He cross sections

In order to determine experimental ^{2}He cross sections, the projected spectra $d^3\sigma/d\Omega_1 d\Omega_2 dE_1$ must be converted to the $(\Omega_{3-12}, \Omega_{12}, \varepsilon)$ coordinate system,[5] where the subscripts 1,2 and 3 denote the two detected particles and the recoil nucleus, respectively. This can be performed by using the Jacobian coordinate transformation

$$\frac{d^3\sigma}{d\Omega_1 d\Omega_2 dE_1} = J \, \frac{d^3\sigma}{d\Omega_{3-12} d\Omega_{12} d\varepsilon} \tag{2}$$

where the Jacobian J is given by[9,5]

$$J = \frac{\partial(\Omega_{3-12}, \Omega_{12}, \varepsilon)}{\partial(\Omega_1, \Omega_2, E_1)} = \frac{1}{\mu_{3-12}\mu_{12}p_{3-12}p_{12}} \, \frac{m_1 m_2 m_3 p_1 p_2}{\left| (m_2+m_3) + \dfrac{m_2(\vec{p}_1-\vec{P})\vec{p}_2}{p_2^2} \right|} , \tag{3}$$

where $\vec{P}$ is the laboratory momentum of the projectile.

In the case of the $(d,{}^2He)$ reaction, $d\Omega_{3-12}$ can be identified as $d\Omega_{^2He}$, the ^2He solid angle in the ^2He-recoil nucleus center-of-mass system, and after integrating Eq. (2) over $d\Omega_{12}$ one obtains for the experimental ^2He cross section for relative energies between ε_ℓ and ε_u

$$\frac{d\sigma_{exp.}}{d\Omega_{^2He}} = \frac{4\pi}{2} \int_{\varepsilon_\ell}^{\varepsilon_u} \frac{1}{J} \left(\frac{d^3\sigma_{exp.}}{d\Omega_1 d\Omega_2 dE_{p_1}} \right) d\varepsilon \quad . \tag{4}$$

The integration over $d\Omega_{12}$ can be performed since the two protons, being in a relative $^1S_0$ state, are emitted isotropically in their c.m. system. The factor of two in the denominator of the right hand side of Eq. (4) corrects for a double counting of pp coincidence events, which arises from the indistinguishability of the two detected particles. The lower and upper integration limits in Eq. (4) must be chosen according to the observable range of ε, which is a function of the detection system geometry, i.e., the angular separation between the two counters, the lower and upper energy cut-offs of the detectors and the ^2He energy. For all the differential cross sections quoted in this work, integration limits of $\varepsilon_\ell = 0.4$ MeV and $\varepsilon_u = 1.0$ MeV were set since for all ^2He energies between 25 and 50 MeV the observable ranges of ε lie within these limits.

C. Discussion of the ^2He energy spectra

Figures 5-7 show representative spectra from the $(d,{}^2He)$ reaction at $E_d = 55$ MeV on targets of ^6Li, ^{10}B and ^{12}C. They will be discussed and compared with existing data from other charge-exchange reactions such as (n,p) and $(t,{}^3He)$. In addition, since these are $T_z = 0$ targets, spectra of the (p,n) and (^{3}He,t) reactions populating the mirror nuclei can also be compared to these (d,^{2}He) results.

1. ^{6}Li(d,^{2}He)^{6}He (Q_o = -4.95 MeV)

Although the ^{6}He nucleus[10] has been studied with particle-transfer as well as charge-exchange reactions (examples of the latter are the ^{6}Li(n,p)^{6}He reaction at E_n = 14 MeV[11] and the ^{6}Li(t,^{3}He)^{6}He reaction at E_t = 22 MeV[12]), only two states have clearly been observed so far, namely the g.s., 0^+, and an excited state at 1.80 MeV with $J^\pi = (2)^+$. Weak evidence for possible broad states at 13.4, 15.3 and 23.2 MeV has been reported in some reactions,[10] but these states have not been seen in any charge-exchange reaction.

At 55 MeV bombarding energy, the ^{6}Li(d,^{2}He)^{6}He reaction enables one to observe an excitation range in ^{6}He up to 25 MeV, thereby permitting a broad search for highly excited levels in the ^{6}He nucleus. Data from this reaction have been taken at 5 laboratory angles between 17-40°. Figure 5 shows a representative ^{2}He energy spectrum measured at Θ_{lab} = 17°. Only the g.s. transition and a fairly weak transition to the 1.80 MeV state were observed. Although the large peak from the ^{1}H(d,^{2}He)n reaction obscures the ^{6}He excitation range from 4 to 8 MeV at this angle, at the other observed angles there is no evidence for ^{6}He levels in this excitation range. The arrows in Fig. 5 indicate the positions of possible transitions to ^{6}He levels which have been previously observed[10] at 13.4, 15.3 and 23.2 MeV. No evidence was obtained for transitions to these states at this or other angles. Similarly to the above (d,^{2}He) reaction, the (p,n)[13] and (^{3}He,t)[14] mirror reactions on ^{6}Li only produce the g.s. and, more weakly, the 1.67-MeV, $(2)^+$ state of ^{6}Be with no evidence for any higher excited states.

2. The ^{10}B(d,^{2}He)^{10}Be Reaction (Q_o = - 2.00 MeV)

The level structure of ^{10}Be has been investigated with a variety of reactions, but no detailed study of this nuclide with a charge-exchange reaction has yet been reported. Data from the ^{10}B(d,^{2}He)^{10}Be reaction were obtained over a laboratory angular range from 17 to 50°. Figure 6 presents a spectrum from this reaction at 40°. Strong transitions to the g.s., 0^+, and to the known[10] 2^+ state at 3.37 MeV were observed. In addition, a strong peak was observed at E_x = 5.96 which could be composed of a mixture of two known states,[10] a 2^+ state at 5.9583 MeV and a 1^- state at 5.9599 MeV. Based on results from investigations[15] of the ^{9}Be(d,p)^{10}Be reaction, the 2^+ state is likely to be the dominant component. Furthermore, there is some evidence for weak (and normally unresolved) transitions to the 7.37-MeV, 3^- and 7.54-MeV, 2^+ states. The highest excitation energy in ^{10}Be at which a transition was observed was found at 9.34 ± 0.10 MeV. This peak is likely to be an unresolved doublet consisting of the 9.27-MeV, (4^-) and the 9.4-MeV, $(2)^+$ states.[10]

Due to the lack of data from other charge-exchange reactions producing ^{10}Be, the present spectra can only be compared with those from reactions populating the mirror nucleus ^{10}C; the latter results were obtained via the (p,n) reaction, which was investigated at E_p = 30 and 50 MeV[16] and the (^{3}He,t) reaction, studied at $E_{^3He}$ = 30 MeV.[17] In all these reactions, only the g.s., 0^+, 3.35-MeV, 2^+ state as well as a presumably 2^+ state at 5.2 MeV in ^{10}C have been observed, which are the analogs of the g.s., 0^+, 3.37-MeV, 2^+ and 5.96-MeV, 2^+ states in ^{10}Be as observed in the (d, ^{2}He) reaction. Although a state at 9.34-MeV was populated with significant strength in the (d, ^{2}He) reaction, its analog in ^{10}C has not yet been identified.

3. $^{12}C(d, ^2He)^{12}B$ (Q_o = - 14.81 MeV)

Figure 7 shows a ^{2}He energy spectrum from the $^{12}C(d, ^2He)^{12}B$ reaction at $\Theta_{lab} = 30°$. At forward angles strong transitions were found to the g.s., 1^+, of ^{12}B. Furthermore a strong peak was observed at $E_x = 4.50 \pm 0.07$ MeV, which consists of unresolved transitions to known states[18] at 4.52 and 4.37 MeV with $J^\pi = 4^-$ and 2^-, respectively. In addition, population of the 0.95-MeV, 2^+ state was observed with moderate strength. The known states at 1.67-MeV, 2^- and 3.39 MeV, 3^- as well as two unresolved states at 5.61-MeV, 3^+ and 5.73-MeV, 3^- were only very weakly populated. Finally, in the spectra obtained at larger angles ($\Theta_{lab} > 35°$), evidence was found for a broad state at $E_x = 8.3 \pm 0.1$ MeV, which cannot be identified with any previously known state.

Similar ^{12}B spectra have been obtained in a study[19] of the $^{12}C(n,p)^{12}B$ reaction at $E_n = 56$ MeV. In addition to the transitions to the g.s., the 0.95-MeV state and the doublet at 4.4 MeV, a somewhat broad peak was observed at $E_x = 7.7 \pm 0.1$ MeV, particularly in the spectra taken at forward angles, with a strength comparable to that of the g.s. transition. Based on its observed energy and width, this state at 7.7 MeV is believed to be the analog of the giant dipole resonance in ^{12}C, which has also been observed in the $^{12}C(\pi^-,\gamma)^{12}B$ reaction[20] at E_x = 8.19 ± 0.5 MeV. It is interesting to note that this state does not significantly appear in the (d,^{2}He) spectra at any angle, which seems to confirm that it is a pure L = 1, S = 0 (Goldhaber-Teller) state.[21] (The (n,p) reaction showed no evidence for transitions to the state observed at 8.3 MeV in the (d,^{2}He) reaction.)

No (t,^{3}He) reaction on ^{12}C has been reported so far. The only other charge-exchange reaction on ^{12}C leading to ^{12}B was performed with the heavy-ion reaction (^{7}Li,^{7}Be) at $E_{^7Li}$ = 52 MeV.[22] Energy spectra obtained in this reaction are similar to those from the (d,^{2}He) reaction, however, no states above E_x = 6 MeV could be observed.

The mirror nucleus ^{12}N has been the subject of several investigations with charge-exchange reactions such as the $^{12}C(p,n)^{12}N$ reaction at E_p= 30 and 50 MeV[16] and the $^{12}C(^3He,t)^{12}N$ reaction at $E_{^3He}$ = 49.3 MeV.[23] The latter study could correlate most states in ^{12}N below 4 MeV with an analog state in ^{12}B with reasonable confidence. For the higher excited states, however, no such assignments could be made; this region does contain several candidates for states analogous to those observed in ^{12}B in the (d,^{2}He) and (n,p) reactions, but additional experimentation is clearly necessary to make any such correlation.

IV. MICROSCOPIC DWBA ANALYSIS

Since detailed structure calculations for the p-shell nuclei investigated herein have been done by Cohen and Kurath,[24] it is possible to perform microscopic DWBA calculations for the (d, ^{2}He) reaction using these wave functions. For the angular distributions leading to the positive parity states of ^{10}Be and ^{12}B shown in Figs. 8 and 9, respectively, the DWBA calculations were carried out utilizing the Oregon State Coupled-Channel Code,[25] whose underlying formalism has been extensively discussed by Madsen.[26]

A characteristic feature of the (d, ^{2}He) reaction is that only the spin-isospin dependent part of the nucleon-nucleon interaction $V_{11}\,(\vec{\sigma}\cdot\vec{\sigma})(\vec{\tau}\cdot\vec{\tau})\,g(r)$ contributes to the transition. For the radial dependence g(r) of the potential, a Yukawa form with an inverse range of 1 fm^{-1} was used. The differential cross section is then an incoherent sum over all allowed values of the orbital and total angular momentum transfer L and J and is given by

$$\frac{d\sigma}{d\Omega} = N\, V_{11}^2 \sum_{LJ} \sigma_{DWBA}^{LJ} \qquad (5)$$

where V_{11} is the interaction strength, here taken to be 12 MeV, a typical value[26] inferred from other reaction studies, and N is a normalization constant which contains all information on the projectile system such as the projectile spectroscopic amplitude and the effects of the spatial extent of the projectile on the interaction strength.[27] Furthermore, the normalization constant takes into account the fact that the experimental cross section does not comprise the entire ^{2}He g.s., but is limited to $0.4 < \varepsilon < 1.0$ MeV. Since intermediate-coupling wave functions were used for the target and residual nuclei, each term σ^{LJ}_{DWBA} in Eq. (5) is a coherent sum over all possible values of the single-particle total angular-momentum quantum numbers j_1 and j_2 of the initial and final nucleus, respectively, with orbital angular-momentum quantum numbers $\ell_1 = \ell_2 = 1$. These contributions were weighted by the spectroscopic amplitudes S which are defined[26] as

$$S(JJ_iJ_f;TT_iT_f;j_1j_2)$$

$$= \frac{1}{(2J+1)^{1/2}(2T+1)^{1/2}} \quad \langle \Phi_{J_fT_f} \| A_{JT} \| \Phi_{J_iT_i} \rangle .$$

They were evaluated by Kurath[28] for the target nuclei ^{10}B and ^{12}C and are listed in Table I.

The single-particle energies of the $p_{3/2}$ and $p_{1/2}$ neutrons and protons were assumed to be the same for the ^{10}B, ^{10}Be, ^{12}C and ^{12}B nuclei. In order to obtain values that are independent of the residual interaction, the $p_{1/2}$ single-particle energies for a neutron $E(\nu p_{1/2})$ and a proton $E(\pi p_{1/2})$ were determined from the binding-energy differences between $^{12}C(g.s.,0^+)$ and $^{13}C(g.s.,1/2^-)$ and between $^{12}C(g.s., 0^+)$ and $^{13}N(g.s., 1/2^-)$, respectively. The values for $E(\nu p_{3/2})$ and $E(\pi p_{3/2})$ were then obtained from the difference between the $p_{3/2}$ and $p_{1/2}$ single-particle energies as used by Cohen and Kurath.[24] The bound-state wave functions were calculated in the usual way with a real Woods-Saxon well with radius R = 2.86 fm, diffuseness a = 0.65 fm and spin-orbit potential $V_{s.o.}$ = 6 MeV. The well depth was adjusted to give the single-particle energies.

The optical model potential parameters to generate the distorted waves were taken from a study[29] of elastic deuteron scattering from ^{12}C at 52 MeV. For the real part a volume Woods-Saxon potential with a well depth V = 71.8 MeV, radius parameter r_v = 1.25 fm and diffuseness a_v = 0.7 fm was used, whereas the absorptive imaginary part consisted of a surface Woods-Saxon potential with W = 11.0 MeV, r_w = 1.25 fm and a_w = 0.7 fm. The same parameter set was used for the entrance and exit channels.

Results from these DWBA calculations of the (d, ^2He) reaction on ^{10}B and ^{12}C are shown as solid curves in Figs. 8 and 9. Each distribution has been individually normalized to the data with the value of the normalization constant N listed in Table II along with the allowed L and J transfer quantum numbers and the label of the spectroscopic amplitudes (Table I) used in the calculations.

For the $^{10}B(d,{}^2He){}^{10}Be$ reaction, the shapes of the theoretical angular distributions are in reasonable agreement with the data. The calculated distributions to the 3.37, 5.96 and 9.4 MeV states, which were all assumed to have $J^\pi = 2^+$ and were obtained with the spectroscopic amplitudes 2^+ a, b and d, respectively, (Table I), are similar in shape except for that to the 5.96 MeV state at forward angles; this variation is probably due to different relative contributions from L=0 and 2 transitions. With regard to the extracted value of the normalization constant N, only that for the 9.4 MeV state differs significantly from the others. Its large value could be a result of a substantial unknown contribution to the data from the unresolved 4^- state at 9.27 MeV. This is consistent with the results from studies[15] of the $^9Be(d,p)^{10}Be$ reaction which populates the 9.27-MeV and 9.4-MeV states with comparable strength. Since the value of N for the 5.96-MeV, 2^+ state does not deviate significantly from that of the g.s. and first excited state, the contribution to the experimental cross section from the 1^- state, which lies only 16 keV higher, seems to be quite small, again in agreement with the findings of $^9Be(d,p)^{10}Be$ reaction studies.[15] Calculations were also carried out using the spectroscopic amplitudes 2^+c. They yielded a distribution similar to that of the 2^+a set but with a magnitude smaller by a factor of $\sim$ 15. Since a known 2^+ state is observed with weak strength at 7.54 MeV, it is likely that the spectroscopic amplitudes 2^+c correspond to this state.

Figure 9 shows the results of the microscopic DWBA analysis for the $^{12}C(d,{}^2He)^{12}B$ reaction leading to the g.s., 1^+ and the 0.95-MeV, 2^+ state. Due to the lack of spectroscopic amplitudes, no calculations were performed for the transitions to the negative parity states, which contain s-d shell configurations. For the g.s. transition, the shape of the calculated angular distribution is in acceptable agreement with the data. The experimental cross section is about five times larger than that of the $^{10}B(d,{}^2He)^{10}Be$ (g.s.) transition. Although the theory predicts correctly a larger value, it is by only a factor of about three. Agreement between the experimental and the calculated distributions is poorer for the pure L = 2 transition to the 0.95-MeV, 2^+ state of ^{12}B. Whereas the experimental distribution falls off rapidly at backward angles, the DWBA calculations predict a distribution that is quite flat between $\Theta_{c.m.} = 30^\circ$ and 70°.

This successful description of the angular distributions of the (d,^{2}He) reaction on targets of ^{10}B and ^{12}C indicates that the assumed direct one-step charge-exchange reaction mechanism is consistent with the data and indicates the potential usefulness of this reaction as a spectroscopic tool. However, preliminary calculations have indicated that the tensor force could be of some importance. Furthermore, exchange effects and multi-step processes such as d-^{3}He-^{2}He may have to be considered as well, before a complete understanding of the mechanism of the (d,^{2}He) reaction can be obtained.

V. SUMMARY AND CONCLUSION

The (d,^{2}He) reaction has been investigated on targets of ^{6}Li, ^{10}B, and ^{12}C at E_d = 55 MeV. A detector arrangement was employed that permitted a kinematically complete coincidence measurement of two protons with small relative energies thereby taking advantage of the enhancement of the cross section due to the pp FSI of the virtual $^1S_0$ g.s. of ^{2}He. Projected proton energy spectra $d^3\sigma/d\Omega_1 d\Omega_2 dE_p$ clearly exhibit this enhancement which is well reproduced by FSI calculations based on the theory of Watson[6] and Migdal.[7] Where comparisons were possible, the ^{2}He energy spectra from reactions on these T_z = 0 targets were found to be quite similar to corresponding spectra obtained from either the analogous charge-exchange reactions (n,p) and (t,^{3}He) or the mirror reactions (p,n) and (^{3}He,t).

Further indication for a charge-exchange mechanism of the (d,^{2}He) reaction was obtained from a microscopic DWBA analysis of the angular distributions from the ^{10}B and ^{12}C targets using spectroscopic amplitudes derived from intermediate-coupling wave functions. Reasonable agreement with the data was obtained both in shape and relative magnitude. Since the (d,^{2}He) reaction always proceeds by spin-flip, it is furthermore an useful complement to other comparable charge-exchange reactions, such as the (n,p) reaction, which in general can take place by spin-flip and non-spin-flip transitions. As shown for the reaction on ^{12}C, a comparison of the energy spectra from these particular two reactions can help identify transitions that proceed by non-spin-flip alone, since they should be observed in the (n,p) but not in the (d,^{2}He) reaction.

ACKNOWLEDGEMENT

We wish to thank Dr. V. R. Brown and Dr. V. A. Madsen for their assistance in performing the DWBA calculations as well as for many valuable discussions. We also thank Dr. D. Kurath for providing the spectroscopic amplitudes. This work was supported by the Nuclear Physics and Nuclear Sciences Divisions of the U. S. Department of Energy under contract No. W-7405-ENG-48.

REFERENCES AND FOOTNOTES

†Present address: Institut für Strahlen-und Kernphysik der Universität Bonn, West Germany.

1. R. Jahn, G. J. Wozniak, D. P. Stahel, and J. Cerny, Phys. Rev. Lett. 37, 812 (1976).
2. H. E. Conzett, E. Shield, R. J. Slobodrian, and S. Yamabe, Phys. Rev. Lett. 13, 625 (1964).
3. R. J. Slobodrian, H. E. Conzett, and F. G. Resmini, Phys. Lett. 27B, 405 (1968).
4. J. C. Davis, J. D. Anderson, S. M. Grimes, and C. Wong, Phys. Rev. C 8, 863 (1973).
5. G. G. Ohlsen, Nucl. Instrum. Methods 37, 240 (1965).
6. K. M. Watson, Phys. Rev. 88, 1163 (1952).
7. A. B. Migdal, Zh. Eksp. Teor. Fiz. 28, 3 (1955) [Sov. Phys. JETP 1, 2 (1955)].
8. E. M. Henley, in Isospin in Nuclear Physics, edited by D. H. Wilkinson, (North-Holland, Amsterdam, 1969) p. 15.
9. J. P. Burq, J. C. Cabrillat, M. Chemarin, B. Ille, and G. Nicolai, Nucl. Phys. A179, 371 (1972).
10. F. Ajzenberg-Selove, Nucl. Phys. A227, 1 (1974).
11. F. Merchez, R. Bouchez, and A. I. Yavin, Nucl. Phys. A182, 428 (1972).
12. R. H. Stokes and P. G. Young, Phys. Rev. C 3, 984 (1971).
13. C. J. Batty, B. E. Bonner, E. Friedman, C. Tschalär, L. E. Williams, A. S. Clough, and J. B. Hunt, Nucl. Phys. A120, 297 (1968).

14. R. W. Givens, M. K. Brussel, and A. I. Yavin, Nucl. Phys. A187, 490 (1972).

15. R. E. Anderson, T. T. Kraushaar, M. E. Rickey, and W. R. Zimmerman, Nucl. Phys. A236, 77 (1974).

S. E. Darden, G. Murillo, and S. Sen, Nucl. Phys. A266, 29 (1976).

16. A. S. Clough, C. J. Batty, B. E. Bonner, and L. E. Williams, Nucl. Phys. A143, 385 (1970).

17. N. Mangelson, F. Ajzenberg-Selove, M. Reed, and C. C. Lu, Nucl. Phys. 88, 137 (1966).

18. F. Ajzenberg-Selove, Nucl. Phys. A248, 1 (1975).

19. F. P. Brady, Crocker Nuclear Laboratory Report No. UCD-CNL 190, 55 (1977) (unpublished). W. M. McNaughton, N. S. P. King, F. P. Brady, and J. L. Ullmann, Nucl. Instrum. Methods 129, 241 (1975).

20. J. A. Bistirlich, K. M. Crowe, A. S. L. Parsons, P. Skarek, and P. Truoel, Phys. Rev. Lett. 25, 689 (1970).

21. F. J. Kelly and H. Überall, Phys Rev. 175, 1235 (1968).

22. G. C. Ball, G. J. Costa, W. G. Davies, J. S. Forster, J. C. Hardy, and A. B. McDonald, Phys. Rev. Lett. 31, 395 (1973).

23. C. F. Maguire, D. L. Hendrie, D. K. Scott, and J. Mahoney, Phys. Rev. C 13, 933 (1976).

24. S. Cohen and D. Kurath, Nucl. Phys. 73, 1 (1965).

25. M. J. Stomp, F. A. Schmittroth, and V. A. Madsen, Oregon State University, Nuclear Physics Group Technical Report (unpublished).

26. V. A. Madsen, in Nuclear Spectroscopy and Reactions, edited by J. Cerny (Academic, New York and London, 1975) Part D, p. 249.

27. J. J. Wesolowski, E. H. Schwarcz, P. G. Roos, and C. A. Ludemann, Phys. Rev. 169, 878 (1968).

28. D. Kurath, private communication. S. Cohen and D. Kurath, Nucl. Phys. A101, 1 (1967).

29. F. Hinterberger, G. Mairle, U. Schmidt-Rohr, G. J. Wagner and P. Turek, Nucl. Phys. A111, 265 (1968).

Table I. Spectroscopic Amplitudes $S(JJ_iJ_f;101;j_1j_2)$. (Ref. 28).

j_2j_1		3/2 3/2			1/2 3/2		3/2 1/2		1/2 1/2
J		3	2	1	2	1	2	1	1
J_f^π	α	i) $A = 10$, $J_i^\pi = 3^+$							
0^+	a	.4136							
2^+	a	−.5364	.4411	−.1351	.2358	.3681	−.0809	−.1390	.0236
	b	.3414	−.1098	.2623	−.1966	.6506	.1191	.0083	−.0312
	c	.0356	−.3775	.3797	.2308	−.0018	−.1080	.3036	.0386
	d	−.2996	−.0581	−.0501	.3889	−.1922	−.0192	−.1513	.1323
		ii) $A = 12$, $J_i^\pi = 0^+$							
1^+	a			.0539		.4881		.2399	.0412
2^+	a		−.0429		−.4808		.0800		

Table II. Summary of the values for the normalization constant N extracted from a DWBA analysis using the spectroscopic amplitudes listed in Table I.

Reaction	E_x	$J_f^{\pi}\alpha$	L	J	N
$^{10}B(d,^{2}He)^{10}Be$	g.s.	$0^{+}a$	2	3	.90
	3.37	$2^{+}a$	0	1	.69
			2	1,2,3	
	5.96	$2^{+}b$	0	1	.74
			2	1,2,3	
	9.4	$2^{+}d$	0	1	3.8
			2	1,2,3	
$^{12}C(d,^{2}He)^{12}B$	g.s.	$1^{+}a$	0,2	1	1.39
	0.95	$2^{+}a$	2	2	1.18

FIGURE CAPTIONS

Fig. 1. Schematic diagram of the ^{2}He detection system.

Fig. 2. Proton-proton time-of-flight difference spectrum from the $^{12}C(d,pp)^{12}B$ (g.s.,1^{+}) reaction at E_d = 55 MeV. See text.

Fig. 3. Two-dimensional proton energy spectrum E_{p_1} vs. E_{p_2} from the $^{12}C(d,pp)^{12}B$ reaction at E_d = 55 MeV. See text.

Fig. 4. Projected E_{p_1} energy spectrum from the $^{12}C(d,pp)^{12}B$ (g.s.,1^{+}) reaction at E_d = 55 MeV. The solid curve represents the result of a Watson-Migdal FSI calculation normalized to the data.

Fig. 5. ^{2}He energy spectrum from the $^{6}Li(d,^{2}He)^{6}He$ reaction at E_d = 55 MeV.

Fig. 6. ^{2}He energy spectrum from the $^{10}B(d,^{2}He)^{10}Be$ reaction at E_d = 55 MeV.

Fig. 7. ^{2}He energy spectrum from the $^{12}C(d,^{2}He)^{12}B$ reaction at E_d = 55 MeV.

Fig. 8. Angular distributions from the $^{10}B(d,^{2}He)^{10}Be$ reaction at E_d = 55 MeV. Statistical error bars are shown. The solid curves are microscopic DWBA calculations normalized to the data.

Fig. 9. Angular distributions from the $^{12}C(d,^{2}He)^{12}B$ reaction at E_d 55 MeV. Statistical error bars are shown. The solid curves are microscopic DWBA calculations normalized to the data.

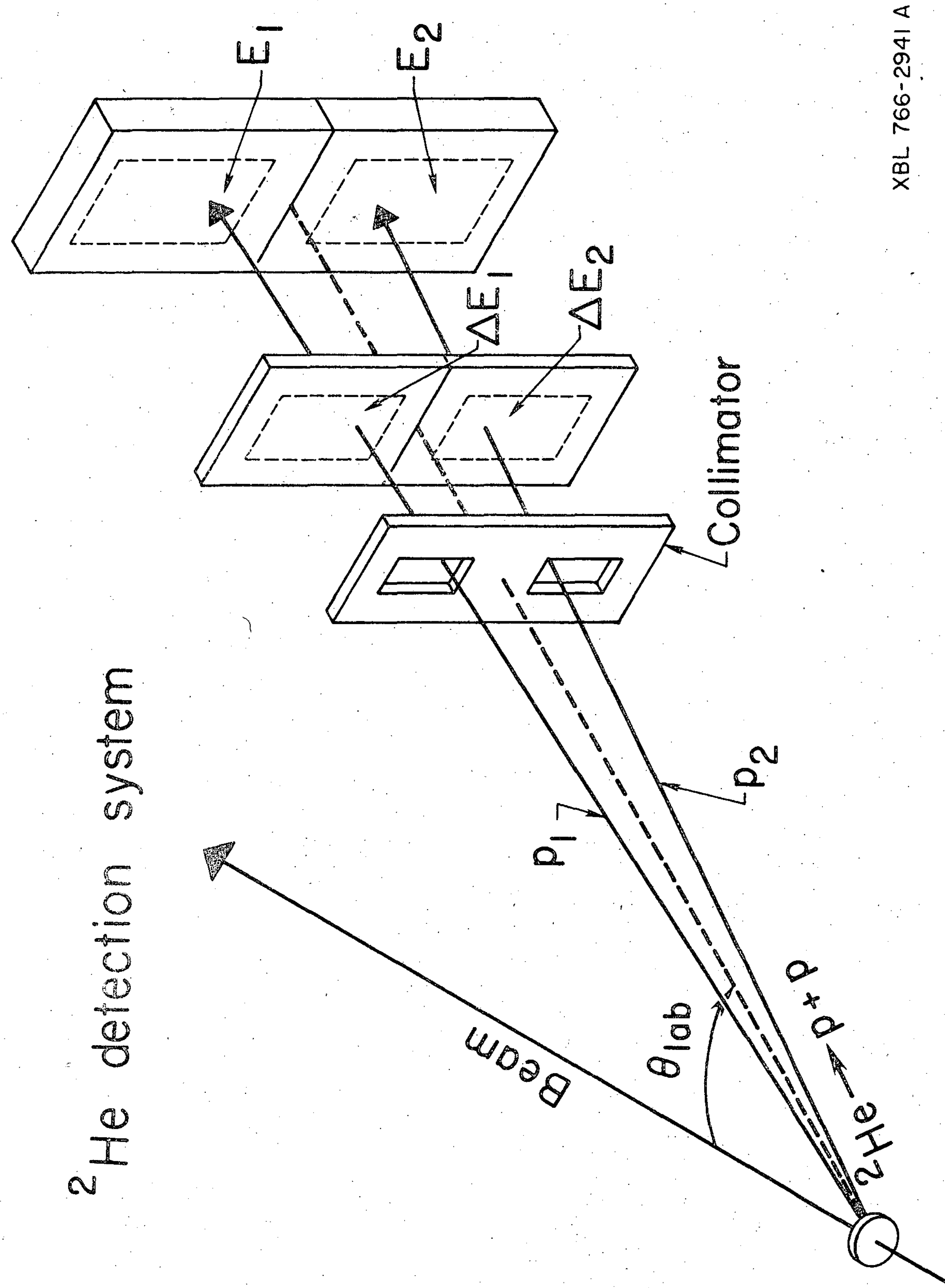
^{2}He detection system
E_1
E_2
ΔE_1
ΔE_2
Collimator
p_1
p_2
Beam
θ_{lab}
$^2He \rightarrow p+p$
XBL 766-2941 A

Fig. 1

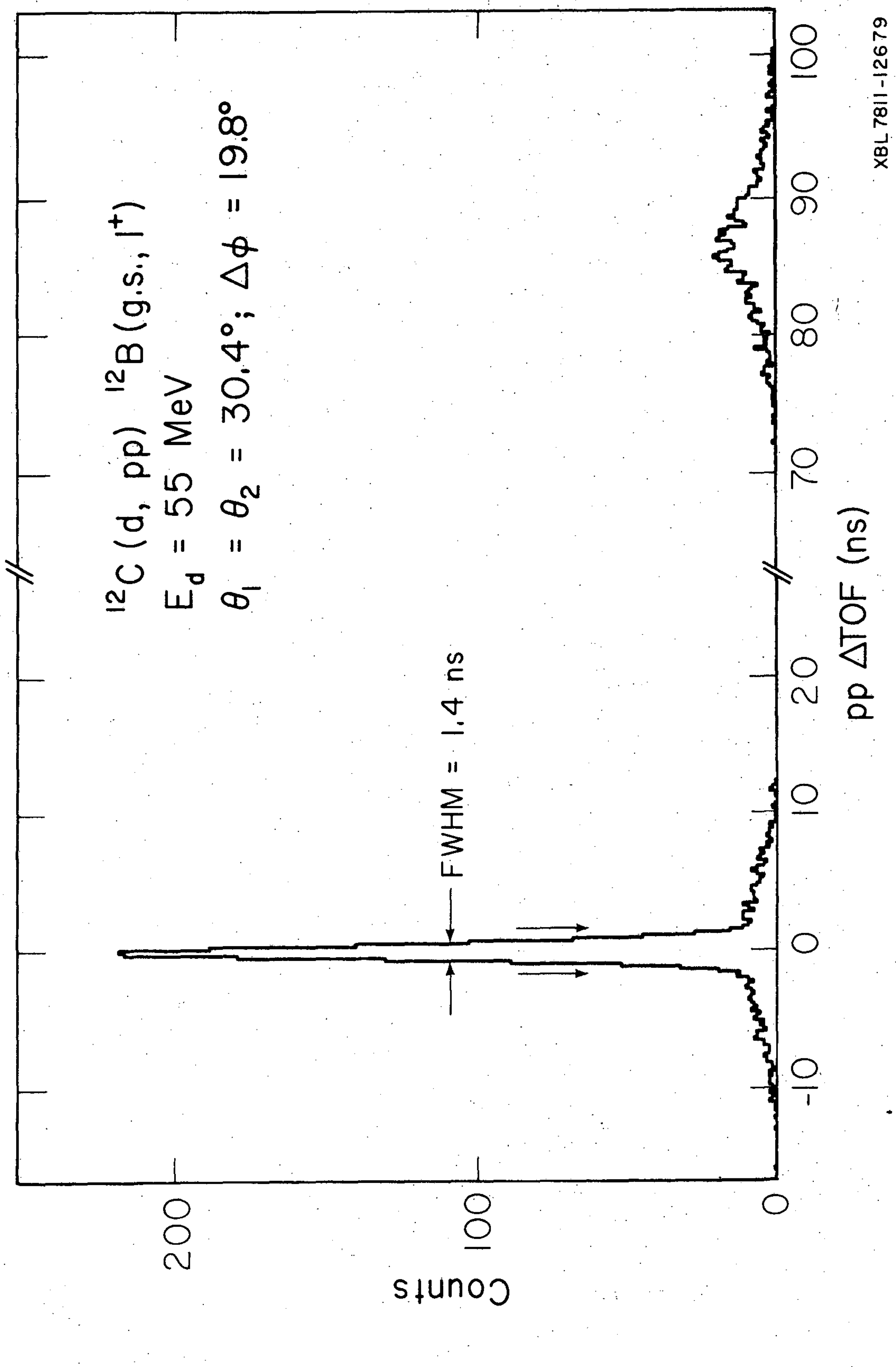

12C (d, pp) 12B (g.s., 1+)
E_d = 55 MeV
θ1 = θ2 = 30.4°; Δφ = 19.8°
FWHM = 1.4 ns
Counts
200
100
0
-10
0
10
20
70
80
90
100
pp ΔTOF (ns)
XBL 7811-12679

Fig. 2

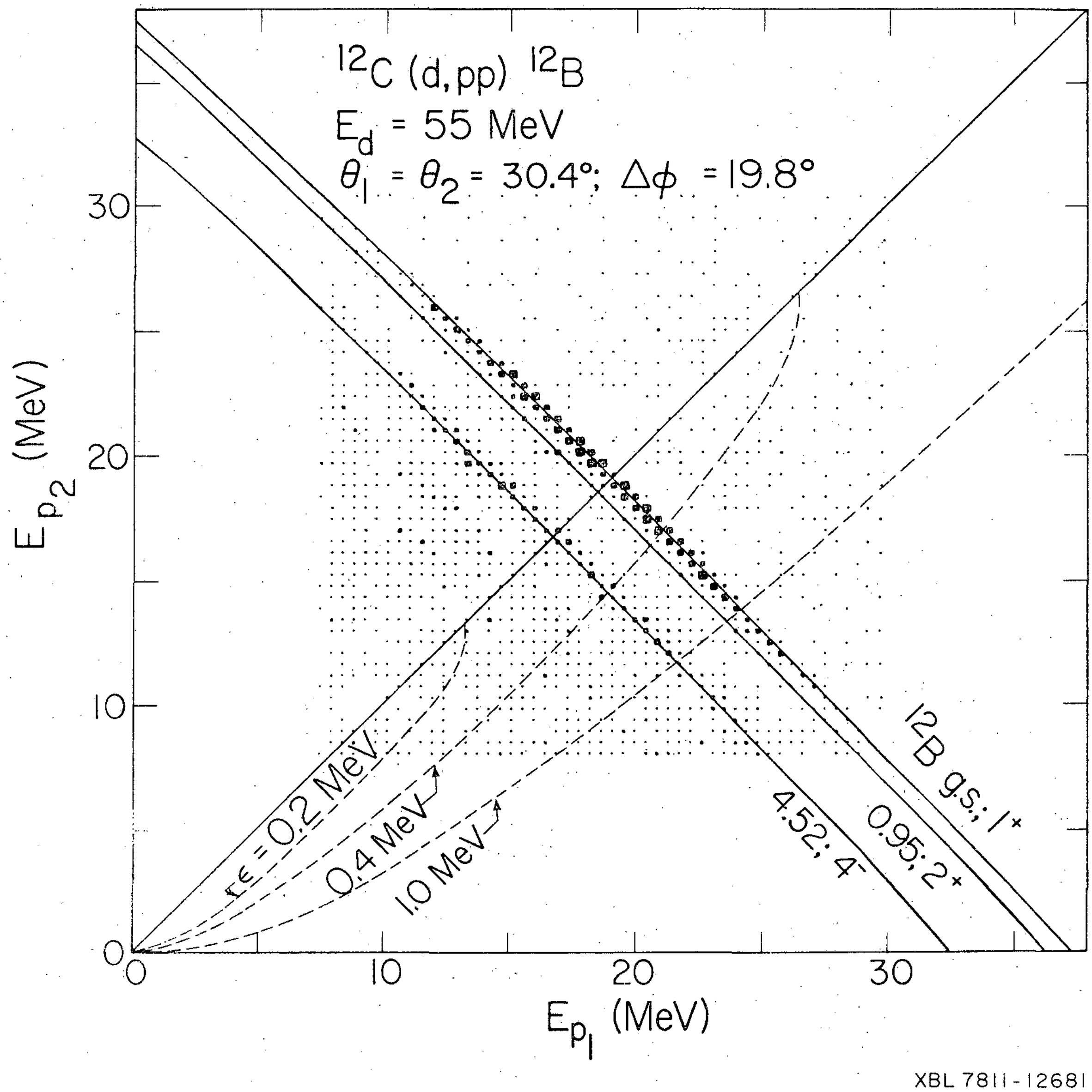

^{12}C (d,pp) ^{12}B
E_d = 55 MeV
$\theta_1 = \theta_2 = 30.4°$; $\Delta\phi$ = 19.8°
E_{p_2} (MeV)
E_{p_1} (MeV)
0
10
20
30
ϵ = 0.2 MeV
0.4 MeV
1.0 MeV
4.52; 4⁻
0.95; 2⁺
^{12}B g.s.; 1⁺
XBL 7811-12681

Fig. 3

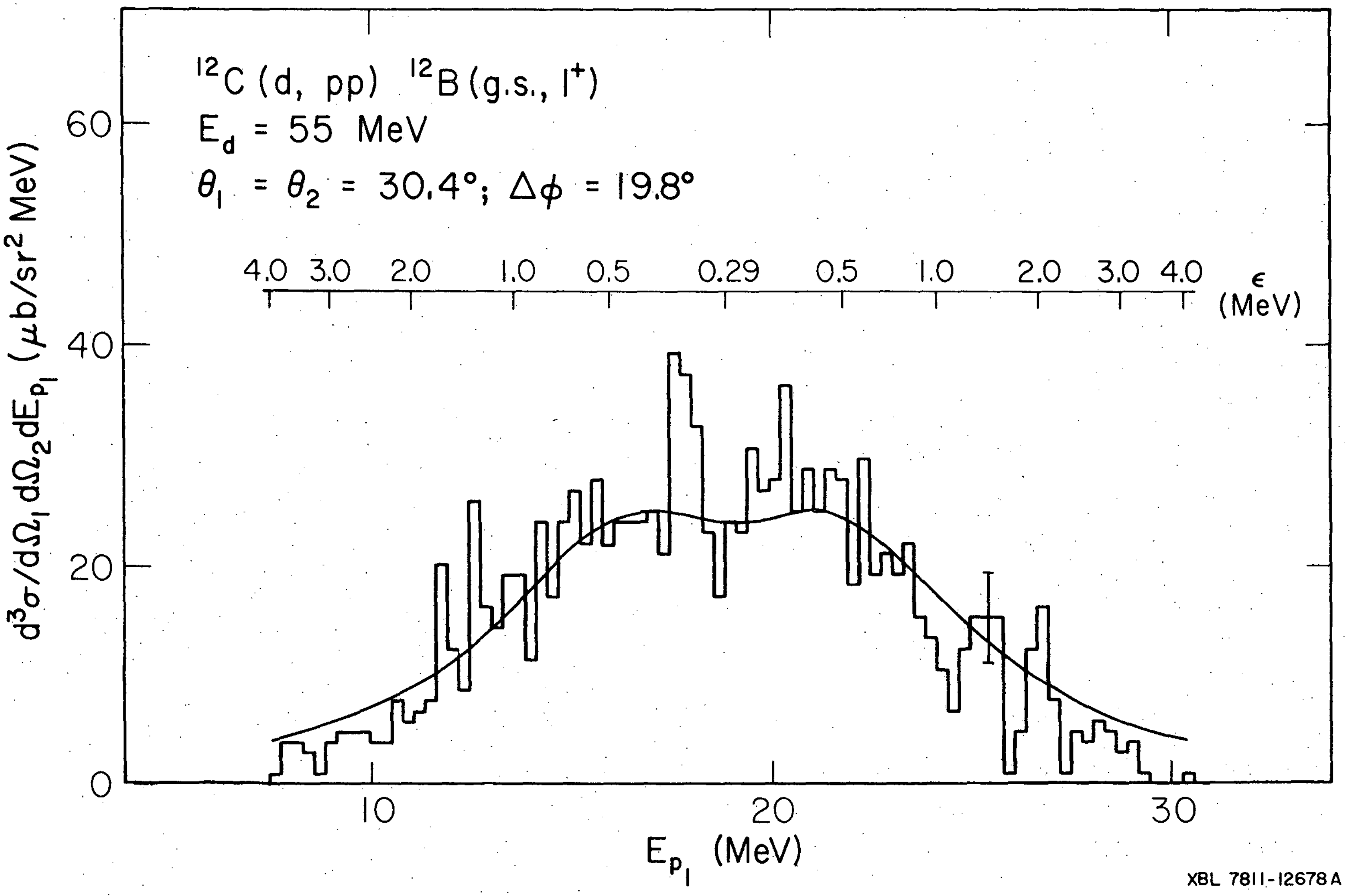

12C (d, pp) 12B (g.s., 1+)
Ed = 55 MeV
θ1 = θ2 = 30.4°; Δφ = 19.8°
4.0 3.0 2.0 1.0 0.5 0.29 0.5 1.0 2.0 3.0 4.0
ε (MeV)
d3σ/dΩ1 dΩ2 dEp1 (μb/sr2 MeV)
60
40
20
0
10
20
30
Ep1 (MeV)
XBL 7811-12678A

Fig. 4

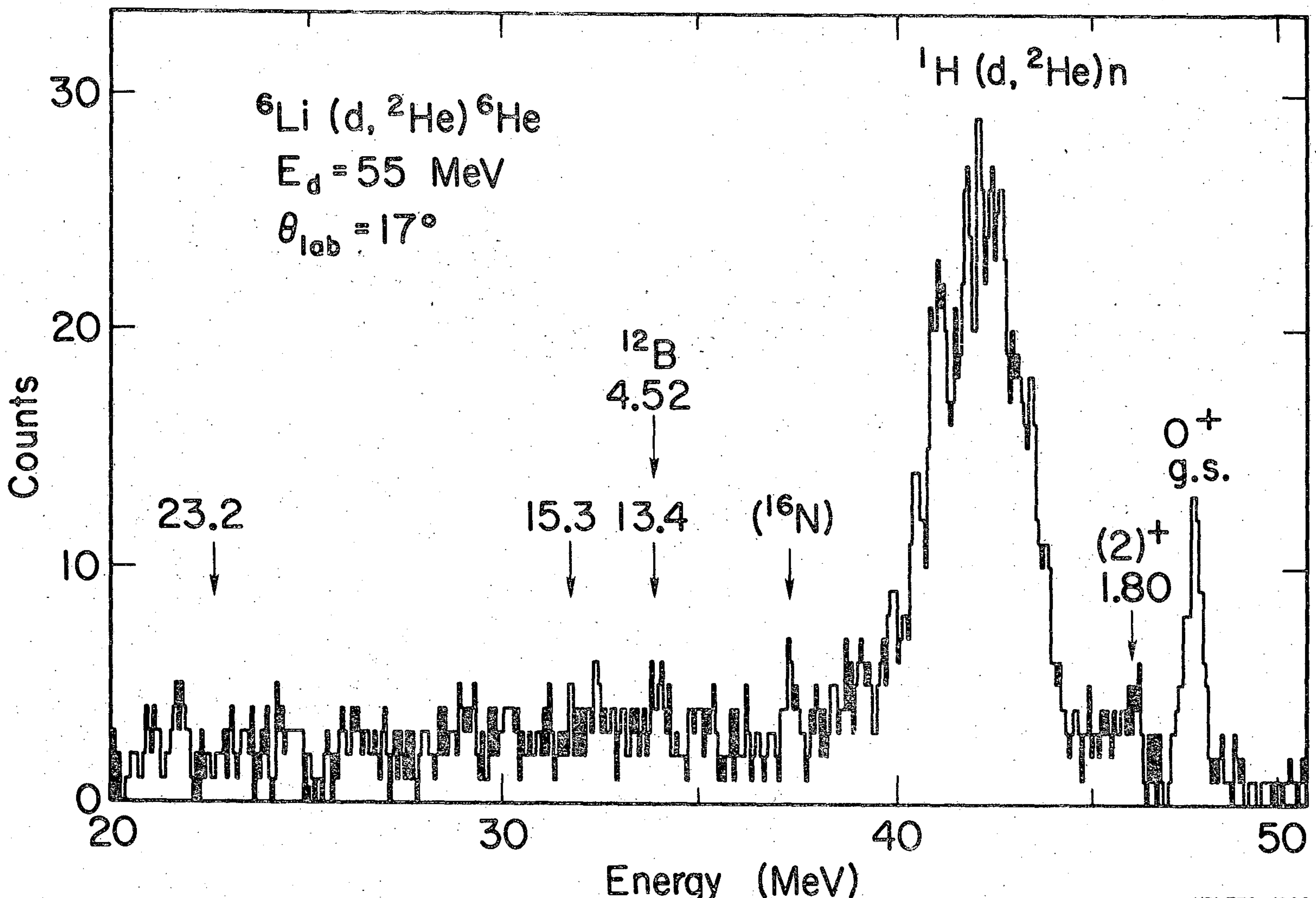

XBL779-1908

Fig. 5

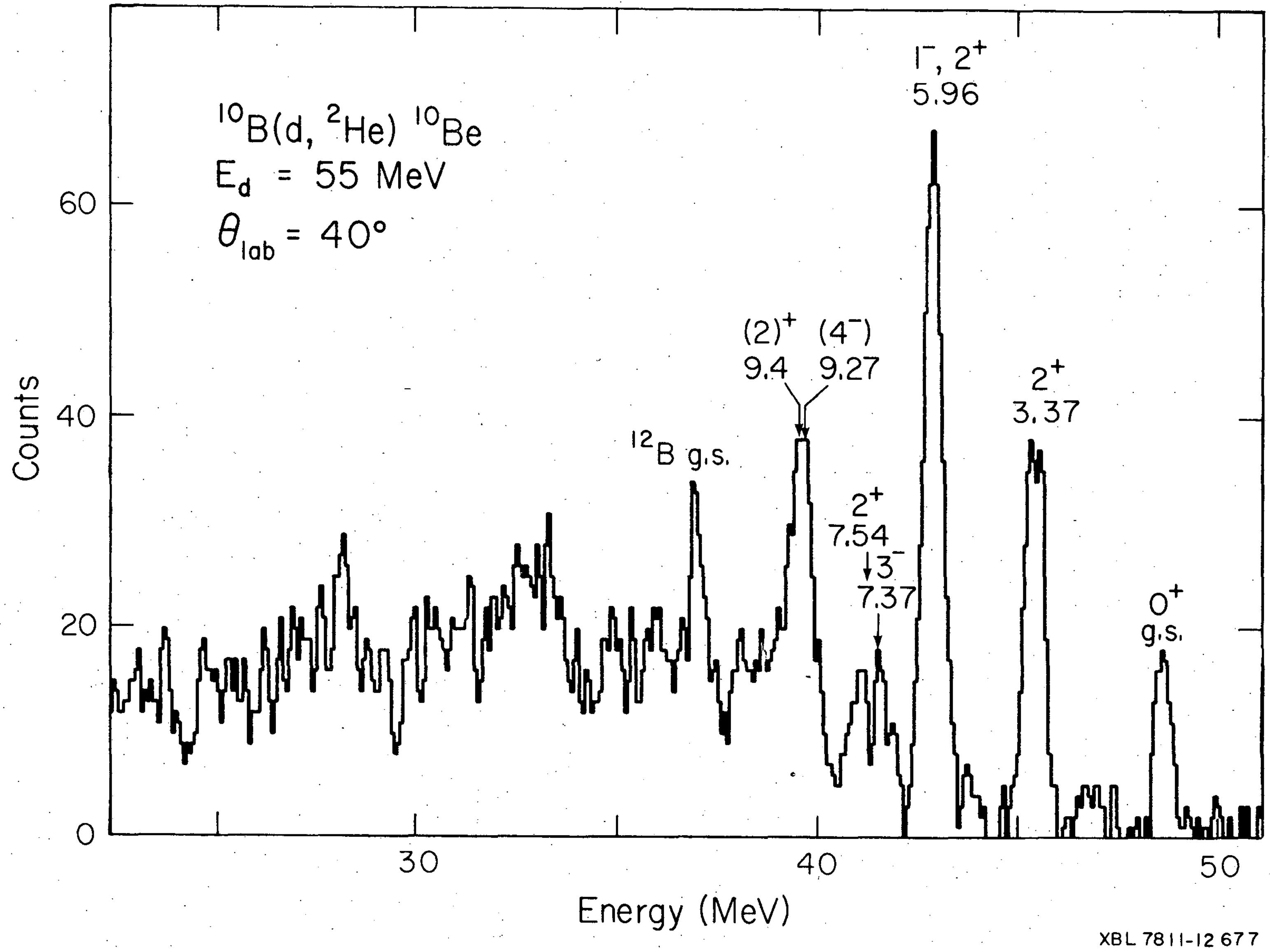

Fig. 6

LBL-8636

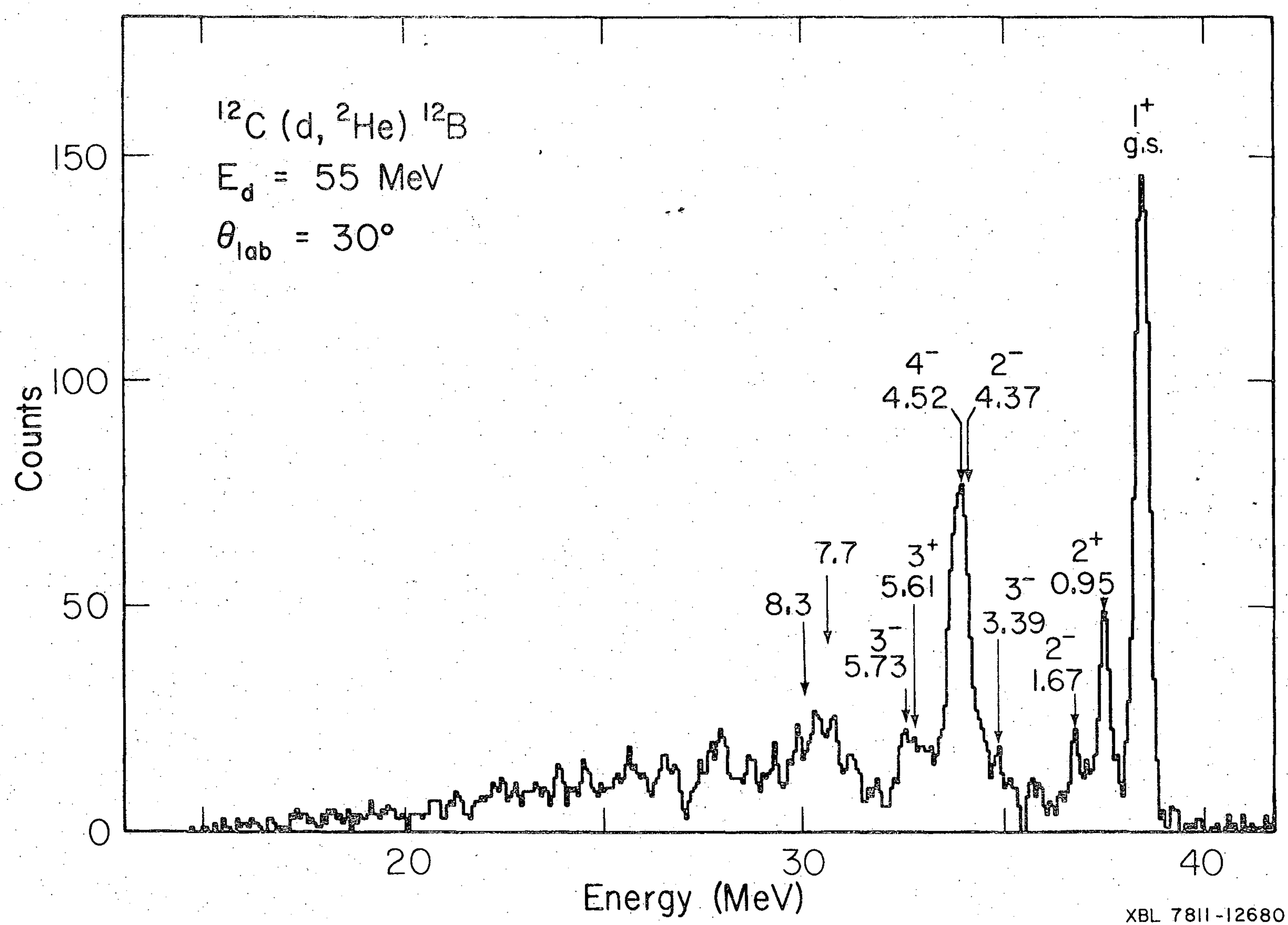
$^{12}C(d, {}^{2}He)\,{}^{12}B$
E_d = 55 MeV
θ_{lab} = 30°
Counts
Energy (MeV)
0
50
100
150
20
30
40
1^+ g.s.
4^- 4.52
2^- 4.37
7.7
8.3
3^+ 5.61
3^- 5.73
3^- 3.39
2^+ 0.95
2^- 1.67
XBL 7811-12680

Fig. 7

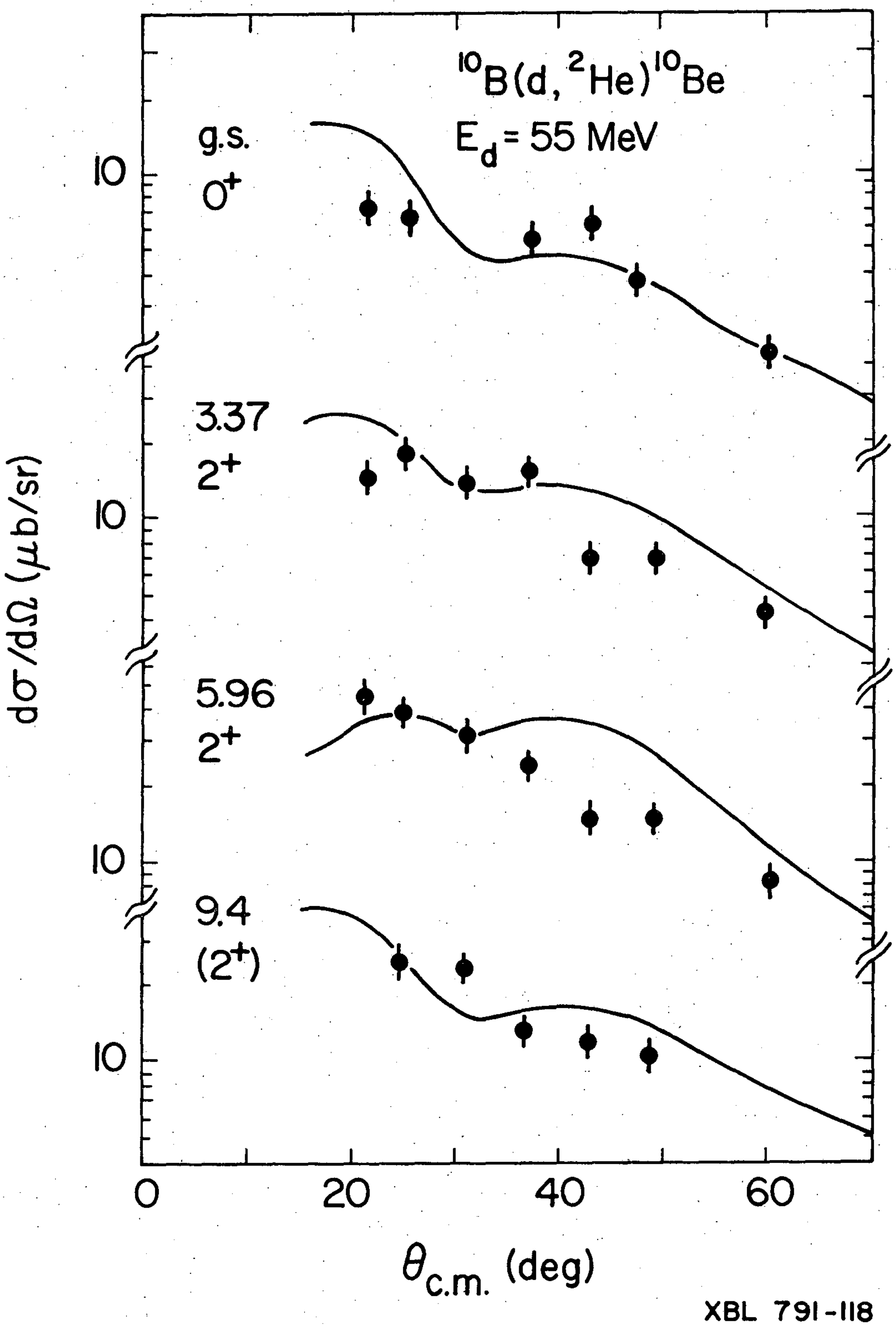
$^{10}B(d,^{2}He)^{10}Be$
E_d = 55 MeV
g.s.
0^+
3.37
2^+
5.96
2^+
9.4
(2^+)
10
10
10
10
dσ/dΩ (μb/sr)
0
20
40
60
$\theta_{c.m.}$ (deg)
XBL 791-118

Fig. 8

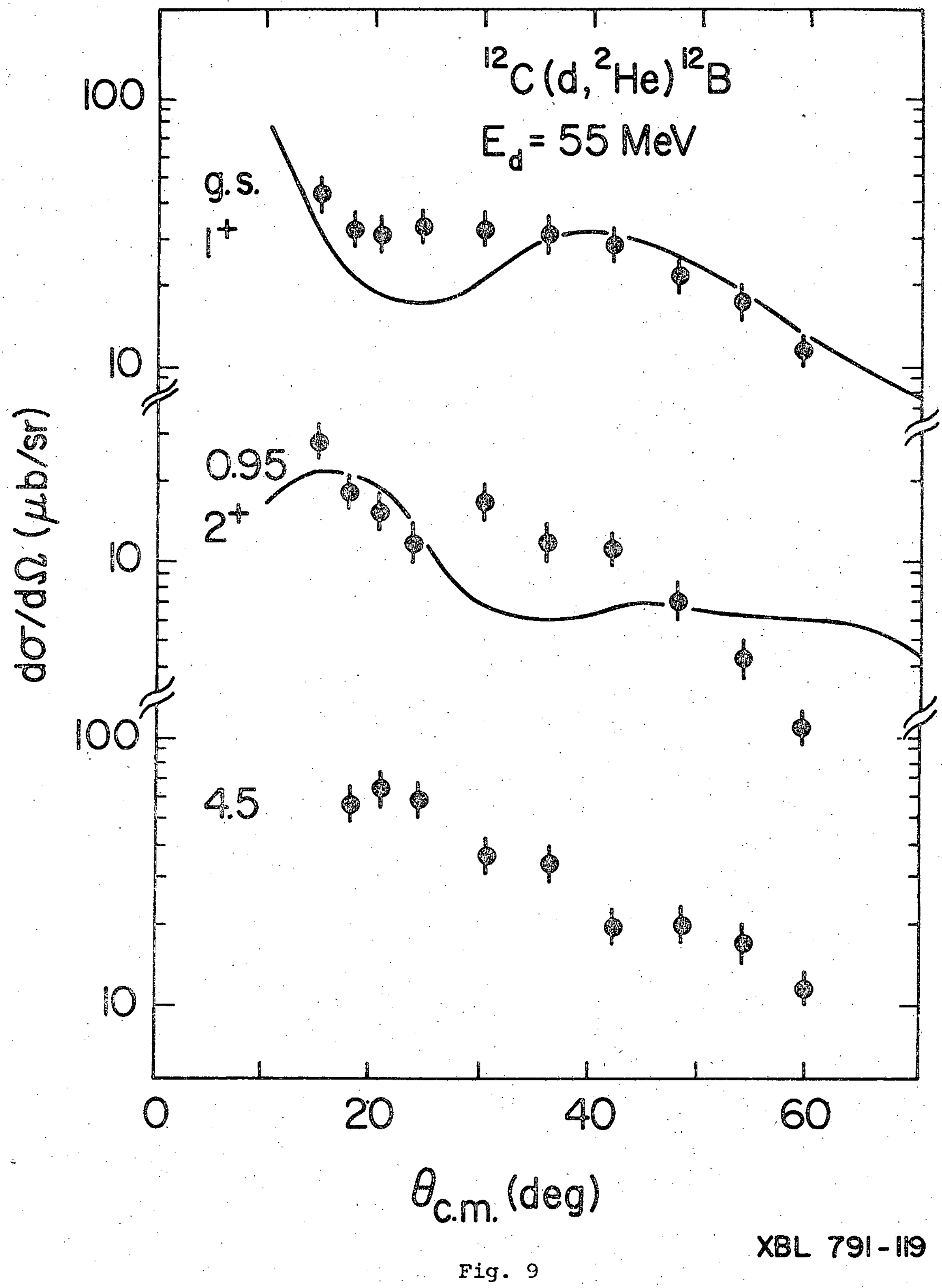

$^{12}C(d,^{2}He)^{12}B$
E_d = 55 MeV
g.s.
1+
0.95
2+
4.5
100
10
100
10
100
10
0
20
40
60
dσ/dΩ (μb/sr)
θc.m. (deg)
XBL 791-119

Fig. 9

TECHNICAL INFORMATION DEPARTMENT
LAWRENCE BERKELEY LABORATORY
UNIVERSITY OF CALIFORNIA
BERKELEY, CALIFORNIA 94720